

# Co-seismic slip of the 18 April 2021 $M_w$ 5.9 Genaveh earthquake in the South Dezful Embayment of Zagros (Iran) and its aftershock sequence

M. Jamalreyhani  <sup>\*1,7</sup>, L. Pousse-Beltran  <sup>2</sup>, M. A. Hassanzadeh  <sup>3</sup>, S. Sadat-Arabi  <sup>4</sup>, E. A. Bergman  <sup>5</sup>, A. Shamszadeh  <sup>6</sup>, S. Arvin  <sup>3</sup>, N. Fariborzi  <sup>3</sup>, A. Songhori  <sup>7</sup>

<sup>1</sup>GFZ German Research Center for Geosciences, Potsdam, Germany., <sup>2</sup>University Grenoble Alpes, University Savoie Mont Blanc, CNRS, IRD, UGE, ISTerre, Grenoble, France., <sup>3</sup>Department of Earth Sciences, Institute for Advanced Studies in Basic Sciences, Zanjan, Iran., <sup>4</sup>Science and Research Branch of Islamic Azad University (SRBI AU), Tehran, Iran, <sup>5</sup>Global Seismological Services, Golden, CO, USA, <sup>6</sup>Department of Earth Sciences, College of Sciences, Shiraz University, Shiraz, Iran, <sup>7</sup>Institute of Geophysics, University of Tehran, Tehran, Iran.

**Author contributions:** *Conceptualization:* M. Jamalreyhani, L. Pousse-Beltran, M. A. Hassanzadeh. *Visualization:* M. Jamalreyhani, L. Pousse-Beltran, M. A. Hassanzadeh, S. Sadat-Arabi, E. A. Bergman, A. Shamszadeh. *Formal Analysis:* M. Jamalreyhani, L. Pousse-Beltran, M. A. Hassanzadeh, S. Sadat-Arabi, E. A. Bergman, A. Shamszadeh, Sh. Arvin, N. Fariborzi, A. Songhori. *Software:* M. Jamalreyhani, L. Pousse-Beltran, M. A. Hassanzadeh, S. Sadat-Arabi, E. A. Bergman. *Validation:* M. Jamalreyhani, L. Pousse-Beltran. *Supervision:* M. Jamalreyhani. *Investigation:* M. Jamalreyhani, L. Pousse-Beltran, E. A. Bergman. *Writing:* M. Jamalreyhani, L. Pousse-Beltran, E. A. Bergman, A. Shamszadeh.

**Abstract** On 2021 April 18, an  $M_w$  5.9 earthquake struck the Genaveh region in the south Dezful embayment of the Zagros, Iran. Here, we investigate the active tectonics of the region, the geometry and slip distribution of the causative fault plane, and its aftershock behavior. We applied a combination of different geodetic and seismological methods (slip distribution inversion of the mainshock using Sentinel-1 Interferometric Synthetic Aperture Radar (InSAR), relocation, and moment tensor inversion of aftershocks and background seismicity of the region). Co-seismic InSAR modeling shows that the slip is confined to the sedimentary cover at depths of 4-7 km with a maximum slip of 1 m and highlights the influence of lithology in the rupture propagation. Moment tensors and centroid depths of aftershocks down to  $M_w$  4 show that the distributed aftershocks sequence is dominated by reverse faulting at centroid depths of 4-10 km. The causative fault is compatible and parallel to the trend of the Gulkhari anticline and the coseismic uplift of the Genaveh earthquake implies that the growth of this particular fold is linked to the fault(s). However, still, due to the absence of surface rupture, the clear relationship between buried faulting and surface folding remains unclear.

**Non-technical summary** We investigate the  $M_w$  5.9 Genaveh earthquake that occurred on 2021 April 18 near the Genaveh harbor in the Persian Gulf, located in the Zagros mountains of Iran. We assess this seismic activity using seismology and space geodetic measurements and models. We discuss the connection between faulting and folding in the region and the causative fault of the Genaveh earthquake. Our results show this earthquake involved a gently NE-dipping fault plane. We found that the mainshock was restricted to depths of between 4-7 with a maximum slip of 1 m within the sedimentary cover. Our results are helpful for hazard and risk assessment of the Genaveh harbor which is an important economic spot in Iran.

Production Editor:  
Gareth Funning  
Handling Editor:  
Yen Joe Tan  
Copy & Layout Editor:  
Kirsty Bayliss

Reviewed by:  
Edwin Nissen and  
anonymous reviewer

Received:  
September 27, 2022  
Accepted:  
April 18, 2023  
Published:  
May 18, 2023

## 1 Introduction

The Zagros Fold-and-Thrust Belt (ZFTB) is a seismically active region of Iran, formed during the collision of the Afro-Arabian continent and the Iranian microcontinent (e.g. Stöcklin, 1968; McQuarrie, 2004; Mouthereau et al., 2012). The region presents one of the youngest continental collision zones on Earth and hosts frequent episodes of moderate to large shallow seismicity (e.g. Talebian and Jackson, 2004; Nissen et al., 2019; Jamalreyhani et al., 2022) (Figure 1). The Zagros changes morphology along and across strike, likely reflecting differences in the sedimentary cover – in particular its overall thickness and the spatial extents of weak, detachment-forming evaporitic layers. However, it's not well understood whether these morphological

changes are reflected in (or perhaps even governed by) differences in the style of earthquake faulting. The advent of InSAR and recent improvements in seismic station coverage have allowed focused studies of major earthquake sequences that can shed light on these questions. A long-standing question in the ZFTB is the extent to which the Precambrian basement and the thick Phanerozoic sedimentary layer participate in the observed seismicity (McQuarrie, 2004; Mouthereau et al., 2007; Talebian and Jackson, 2004; Jamalreyhani et al., 2022). Nissen et al. (2011) suggested a vertical separation of the seismicity in the Zagros, implying that most of the moderately-sized events ( $M_w$  5-6), especially those in the ZSFB, happen in the competent segment of the sedimentary layer and most the aftershocks in the basement, mostly triggered by stress perturbations. Recent studies show the variety of deformation styles

\*Corresponding author: m.jamalreyhani@gmail.com

and seismicity in different parts of the ZFTB (e.g. Nissen et al., 2019; Jamalreyhani et al., 2019, 2022, 2021b). The outer part of the ZFTB, named Zagros Foreland Folded Belt (ZFFB), is subdivided into four tectono-stratigraphy domains (Figure 1): from SE to NW, the Fars Arc, the Dezful Embayment, the Lurestan Arc, and the Kirkuk Embayment. Recent studies of earthquakes in the SE Zagros (Qeshm (Nissen et al., 2010), Fin (Roustaei et al., 2010), Khaki-Shonbe (Elliott et al., 2015), Khalili (Jamalreyhani et al., 2021a)) and in the NW Zagros (Ezgeleh and Sarpolzahab (Nissen et al., 2019; Jamalreyhani et al., 2022), Mandali (Nissen et al., 2019), Murmuri (Copley et al., 2015)) have illuminated the structural style in those regions, but so far there has been an absence of large events in the central Zagros. The  $M_w$  5.9 Genaveh earthquake on 2021 April 18, therefore, fills an important gap and provides an opportunity to study the characteristics of observed seismicity in the Dezful Embayment.

The Dezful Embayment, known as the lower-lying area in Zagros ZFFB (Allen and Talebian, 2011), is the ~500 km-long segment situated in the outer part of the central Zagros and covers an area of 75000 km<sup>2</sup> (Allen and Talebian, 2011) (Figure 1). It contains a > 5 km thick of the Fars Group sediments (Figure S1; Gachsaran, Mishan, Aghajari, and Bakhtiyari formations) (Abdullahie Fard et al., 2011; Shamszadeh et al., 2022a). This region is co-located with 45 natural oil fields, equal to ~8% of Earth's total (Najafi et al., 2014; Seraj et al., 2020; Najafi and Lajmorak, 2020; Shamszadeh et al., 2022a) (Figure 1). It is formed from the west of the Kazerun fault zone to the Balarud fault zone in the northwest and in the footwall of the Mountain Front Flexure (MFF) (Berberian, 1995; Allen and Talebian, 2011; Shamszadeh et al., 2022a). Most of the Dezful Embayment arc's seismicity occurs on ~30°-50° dipping blind reverse faults and some on strike-slip mechanisms (Figure 1). In the Dezful Embayment, layer-parallel shortening resulting from the Zagros orogeny is accommodated by several symmetric and asymmetric mostly NW-SE trending anticlines and synclines (Figure 1) (e.g. Sherkati et al., 2006; Seraj et al., 2020).

Almost 7-12 km of the Phanerozoic sedimentary succession including alternative competent and incompetent layers, is folding and faulting in response to the continental collision in the ZFTB (Alavi, 2008; Irandoust et al., 2022). The Precambrian-Cambrian Hormuz salt layer is located between the basement and sediments in ZFFB. Despite some outcrops of Hormuz salt being observed in the adjacent area of the Dezful Embayment, the fold style and geometry suggest a decollement layer at the base of the sedimentary cover in the South Dezful Embayment (SDE) (Shamszadeh et al., 2022a,b, and references therein). Nonetheless, the surface salt diapirs are lacking in the Dezful Embayment (Jahani et al., 2009; Sherkati and Letouzey, 2004; Najafi and Lajmorak, 2020). This challenges the clear exposure of the Hormuz salt layer in the Dezful Embayment (Sherkati and Letouzey, 2004; Jahani et al., 2017) but the lower Paleozoic Shale at depth of ~3-4 km has been reported (Sherkati and Letouzey, 2004; Farahzadi et al., 2019; Najafi and Lajmorak, 2020). The estimated thickness of

the sedimentary cover from subsurface investigations shows ~8-12 km of sediment in the SDE (Sherkati et al., 2006; Najafi and Lajmorak, 2020; Shamszadeh et al., 2022a). This is suggested by the construction of some longitudinal sections along the strike of anticlinal structures and across the NNE-SSW trending, e.g. Kharg-Mish Paleo High (KMPH) (Sherkati et al., 2006; Shamszadeh et al., 2022a). Above the Precambrian crystalline basement, a 4–6 km thick sequence which has been named as 'Competent Group' is composed (Vergés et al., 2011; Najafi and Lajmorak, 2020). Mainly two sets of faults with the NW-SE Zagros trend and the NNE-SSW Afro-Arabian trend have been developed and involved in the deformation of the SDE (e.g. Sepehr and Cosgrove, 2004; Shamszadeh et al., 2022b). In addition to several NW-SE pre-existing basement faults in the ZFTB (e.g. the MFF), most of the SDE's anticlinal structures (e.g. Gulkhari and Gachsaran anticlines) with steeper SW forelimbs are developed over an NW-SE trending emergent or blind thrust faults dipping NE (e.g. McQuarrie, 2004; Carruba et al., 2006). Furthermore, several NNE-SSW trending basement-involved faults, e.g. Kharg-Mish and Hendijan-Bahregansar-Norooz, affected the tectono-stratigraphy evolution of the SDE during the Phanerozoic (Figure 1) (Sherkati and Letouzey, 2004; Abdullahie Fard et al., 2011; Shamszadeh et al., 2022a).

On 2021 April 18, at 6:41 UTC the  $M_w$  5.9 Genaveh earthquake (named after a nearby famous harbor in the Persian Gulf) occurred in the southern portion of the SDE (Figure 1). It was followed by 370 aftershocks larger than  $M_n$  2.5 and 21 aftershocks larger than  $M_n$  4 (Iranian Seismological Center (IRSC) bulletin). This earthquake is an excellent case study of buried thrust faulting in the sedimentary cover of the SDE that could provide valuable information on the subsurface structure of the area. The Genaveh earthquake and its aftershock activity affected the Bushehr province (Tourani et al., 2021) but there are no reports of death due to this event (Tourani et al., 2021). There are no historical and instrumental records of any earthquake unambiguously linked to faults within Bushehr province (Ambraseys and Melville, 1982; Berberian, 1995). The Genaveh seismic cluster partially filled the data gap in the Karasözen et al. (2019) study, in which they relocate the 70-year instrumentally recorded seismicity in the entire Zagros, but there was no report of relocated events in our study area. Nevertheless, the IRSC catalog indicates 3 events larger than  $M_w$  5, co-located with the Gulkhari anticline, and in this study considered as the background seismicity.

Thanks to high-quality satellite data before and after the mainshock, and co- and post-seismic waveform records (both for mainshock and aftershocks), we focus on understanding whether the growth of the Gulkhari anticline is controlled by a fault directly beneath it or not. We probe links between faulting and folding and investigate the robustness of the vertical separation idea, suggested by Nissen et al. (2011). Another important question to answer is which fault or faults are responsible for the shaking. Furthermore, the Genaveh earthquake co-located with the major active Gulkhari

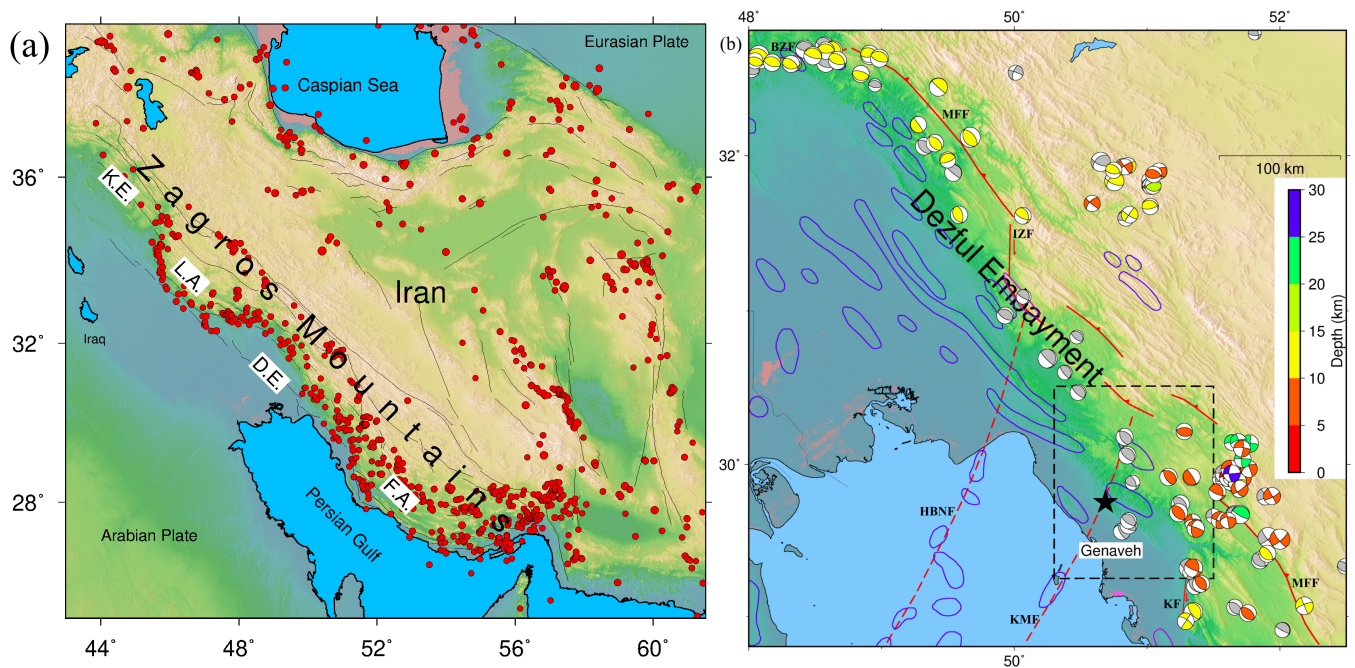


**Figure 1** a) Seismicity of Iran and the location of the Zagros Mountains. Red circles are  $M_w > 5.0$  earthquakes from 1900 to 2020 from the USGS catalog. The black lines represent the major active faults of Iran. Four tectono-stratigraphy domains: from SE to NW, the Fars Arc (F.A.), the Dezful Embayment (D.E.), the Lurestan Arc (L.A.), and the Kirkuk Embayment (K.E.). b) A zoom-in of the Dezful Embayment. The oil fields are shown by blue polygons in this area (Najafi and Lajmorak, 2020). Red lines show major mapped active faults, including the Mountain Front Flexure (MFF) (Berberian, 1995), Kharg-Mish Fault (KMF), Hendijan-Bahregansar Nowrooz Fault (HBNF), Izeh Fault Zone (IFZ), BalaRud Fault Zone (BFZ), and Kazerun Fault (KF). Focal mechanisms from published waveform modeling studies are plotted at relocated epicenters and colored according to focal depth (Karasözen et al., 2019). Those with gray color are from Yaghoubi et al. (2021) without showing depth. The black rectangle shows our study area and the black star shows the location of the 5.9  $M_w$  2021 Genaveh earthquake (Figure 2).

oil field, raising the possibility that this earthquake is induced by human activity. We check the feasible relationship between the exploitation of oil reservoirs with this earthquake. The coseismic slip distribution of the Genaveh earthquake has been investigated by Golshadi et al. (2022) and Jafari et al. (2023) based on Interferometric Synthetic Aperture Radar (InSAR) modeling and they only discuss the mainshock causative fault plane. In this study, we applied a combination of different seismological methods, including relocation of aftershocks using phase readings of local and regional seismic stations, moment tensor inversion of the mainshock, and aftershocks down to  $M_n$  4 using regional waveform records of Iran seismic networks, and slip distribution of the mainshock using Sentinel-1 data.

Our results reveal a close relationship between coseismic uplift and the growth of Gulkhari anticline. We show the seismicity and causative fault are parallel to the trend of the Gulkhari anticline with complex fault zone architecture. Because of the absence of surface rupture, the clear relationship between buried faulting and surface folding remains debated. Our results are helpful for hazard and risk assessment of the Genaveh harbor and surrounding area—one of the important economic spots of Iran.

## 2 The 2021 Genaveh earthquake sequence

### 2.1 Relocation of the sequence

To refine the seismicity patterns we applied the multiple-relocation method “mloc” which is specialized to provide (given suitable data) hypocenters with minimal bias from unknown Earth structures, and realistic uncertainties (Bergman et al., 2022). This technique has been used in relocating many earthquakes in the Zagros and other regions of Iran (e.g., Nissen et al., 2019; Walker et al., 2011; Karasözen et al., 2019; Jamalreyhani et al., 2021a). Thanks to the local and regional seismic networks of the IRSC and the International Institute of Earthquake Engineering and Seismology (IIEES) (Figure 2), we were able to improve the relative locations of the Genaveh seismic sequence and calibrate the absolute location of the cluster with an epicentral uncertainty of 3.1–3.5 km (Figure 2). The relocated cluster includes 117 earthquakes (Table S1), from early 2015 to January 2022, selected on the basis of the number of phase readings and the azimuthal gap. The minimum number of readings for events that are connected to other events, and thus used to estimate relative locations, is 24. The minimum and maximum azimuthal gaps are 19.5° and 163.7°, respectively. There are 69 relocated events soon after the mainshock but some of them are spatially away from the mainshock and likely represent background seismicity. Due to the lack of perma-

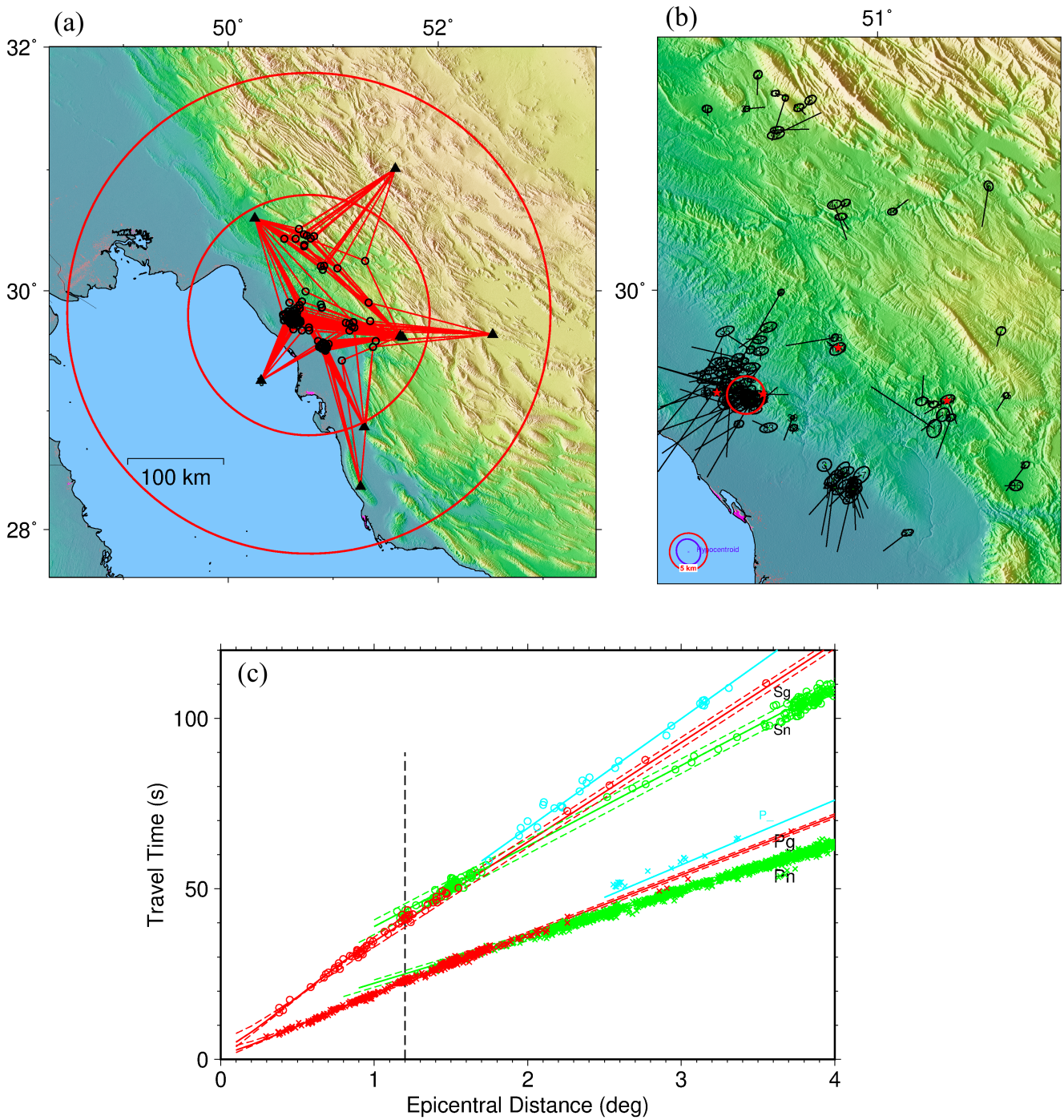


**Figure 2** (a) Station distribution (black triangles) and ray paths (red straight lines) used to determine the calibrated hypocentroid (i.e., absolute location) of the Genaveh cluster. Only observations within  $1.2^\circ$  are used for this purpose. All events in the cluster are plotted, including the 13 events that do not have any readings in that distance range. Large red circles show radii of  $1.0^\circ$  and  $2.0^\circ$  from the cluster hypocentroid. (b) Relocated earthquake hypocenters with 90% confidence ellipses for relative location. The 90% confidence ellipse for the absolute location of hypocentroid is shown as a blue ellipse on the left bottom corner of the figure. The red ellipse represents a reference circle of 5 km radius. The full epicentral uncertainty of any given event requires the addition of relative uncertainty to the hypocentroidal uncertainty. Red stars denote events with a magnitude larger than 5. Black vectors for each event show the change in location from the epicenter given in the arrival time data file, which varies from event to event. (c) Fit between observed phase arrivals (Pg: red crosses, Sg: red circles, Pn: green crosses, Sn: green circles) and theoretical travel times (red and green lines) calculated from the simple flat-layered velocity model determined for this dataset, for epicentral distances of up to  $4^\circ$ . The vertical dashed line at  $1.2^\circ$  indicates the cut-off distance used in the calibrated location of the hypocentroid (228 readings).

ment seismic stations in this region, no near-source data is available for this cluster; the nearest readings are ~30

km away. Focal depths of most events in the cluster are set manually and fixed in the relocation according to the

fit of local distance data (first-arriving Pg and Sg) and a crustal model typical of the Zagros region from other relocation studies, a method with poorer resolving power than near-source readings, but still useful. Due to the lack of appropriate data, we fix the depth of three events at the centroid depth obtained from waveform modeling (see Section 2.2) and in nine cases the focal depths were fixed at 12 km, the median of constrained focal depths for this cluster, and very typical of Zagros earthquakes (e.g. Karasözen et al., 2019). To predict theoretical travel times (Figure 2a), we use a 2 layered crustal model (Moho depth 47 km), in combination with the AK135 model (Table S2). Figure 2 shows the station distribution and ray paths used to relocate the Genaveh seismic sequence and background seismicity, and the pattern and uncertainty of the relative locations. Both Pg and Sg phases have near-zero mean and there is no evidence of a slope with distance to the residuals. The scatter is typical in a region that certainly has some heterogeneity in crustal velocities. The only drawback is the lack of really close-in data, which hampers depth constraints. The 90% confidence ellipse of the hypocenter has semi-axis lengths of 3.1 and 3.5 km and the relative locations, as seen in Figure 2b, are very well constrained.

## 2.2 Moment tensor inversion of the sequence

The temporal evolution of the Genaveh earthquake sequence depicts a mainshock aftershock behavior, including 22 aftershocks larger than 4 within 5 months (Figure 3). During 2015-2020 and before the Genaveh earthquake mainshock, there are 3 events larger than  $M_w$  5 in the southeast of Gulkhari anticline considered as the background seismicity (Figure 3). Seismic records of the Genaveh earthquake sequence and background seismicity were recorded with a good signal-to-noise ratio by broadband sensors at regional distances. Thus, we estimate the centroid Moment Tensor (MT), based on the inversion of regional data. In this distance, modeling has been performed in the frequency band 0.02-0.05 Hz, representing dominant periods of the Rayleigh and Love waves. The MT inversion is based on broadband data of IRSC and IIEES and simultaneously fitting 3-component waveforms in the time and in frequency domains (Figure S2). The observations have been revised manually to exclude noisy records and have been restituted to displacement. To perform centroid MT inversions of the Genaveh earthquake, its aftershocks down to  $M_w$  4, and background seismicity down to  $M_w$  5, we use a probabilistic Bayesian bootstrap optimization nonlinear inversion method (Heimann et al., 2017), which provides ensembles of best-fitting MTs, and estimates the uncertainties and trade-offs for all inverted source parameters. This technique previously has been successfully applied to other earthquakes in the Zagros (Jamalreyhani et al., 2021a, 2022) as well as in other regions (Jamalreyhani et al., 2020; Büyükakpinar et al., 2021; Wang et al., 2022).

Synthetic seismograms are computed using pre-calculated Green's functions (Heimann et al., 2019). The pre-calculated Green's functions were calculated

on a grid for combinations of source depth and source-receiver surface distance based on the regional velocity model "Karbaas" by Karasözen et al. (2019).

Our results for the focal mechanism of the mainshock show that the causative fault plane has a either strike of  $306^\circ \pm 5^\circ$ , a dip of  $28^\circ \pm 9^\circ$ , with a reverse mechanism (rake  $86^\circ \pm 10^\circ$ ), or strike of  $131^\circ \pm 5^\circ$ , a dip of  $62^\circ \pm 4^\circ$ , and rake of  $92^\circ \pm 5^\circ$ , within 68% of confidence (Table S3, Figure S3). All fault plane angles are very well resolved with uncertainties not exceeding  $10^\circ$ . We also determined a shallow centroid depth of  $6 \pm 2$  km and a moment magnitude of  $M_w$  5.9. The obtained focal mechanisms for the mainshock are in good agreement with the Global Centroid Moment Tensor (GCMT) and other available solutions (Table S3). For the smaller magnitude aftershocks, no solution is available to compare. All obtained source parameters for the studied events, together with their uncertainties (68% confidence intervals) are listed in Table S4. We observe almost the same types of focal mechanisms for the aftershocks; the reverse/thrust mechanisms which are located on both sides of the Gulkhari anticline (Figure 3). A combination of seismic section and focal mechanism solutions manifests the faulting and folding at the sedimentary cover (Figure 3).

Figure 4 shows the full moment tensor inversion result of the  $M_w$  5.9 Genaveh earthquake and its decomposition into ISotropic (ISO), Compensated Linear Vector Dipole (CLVD), and Double Couple (DC) parts. A relatively large CLVD component, similar to that resolved independently by GCMT is observed for the mainshock. Resolving non-DC components in MT inversion is challenging (e.g., Zahradnik et al., 2008; Wang et al., 2018; Jamalreyhani et al., 2021b). To exclude that the non-DC is not a result of mismodeling, we evaluate the influence of frequency bands, input data types, and Green functions on non-DC components, and we find the stable non-DC components of the mainshock. However, the accurate resolving of non-DC requires a more detailed 3D-velocity model (Donner et al., 2018; Jamalreyhani et al., 2021b), which is not available for the region. For aftershocks, that are smaller, the double-couple approach is used.

## 2.3 Slip distribution of the 18 April 2021 $M_w$ 5.9 Genaveh earthquake by InSAR modeling

To estimate the slip distribution and fault geometry of the Genaveh earthquake, we rely on near-field geodetic data. The coseismic surface displacement field of the Genaveh mainshock was recorded by the Sentinel-1 from European Space Agency (ESA) in both descending and ascending orbits. We calculated two twelve-day interferograms capturing the mainshock and a few days of post-seismic (8 days on the ascending track A101 and 4 days on the descending track D35, see detail in Table 1). Both interferograms recorded 8 events of  $4 < M_n < 4.6$  after the mainshock. We applied the same methodology as described in Pousse-Beltran et al. (2020) and Jamalreyhani et al. (2021a) for interferograms. The wrapped interferograms were processed with GDM-SAR online service and then were unwrapped using the branch

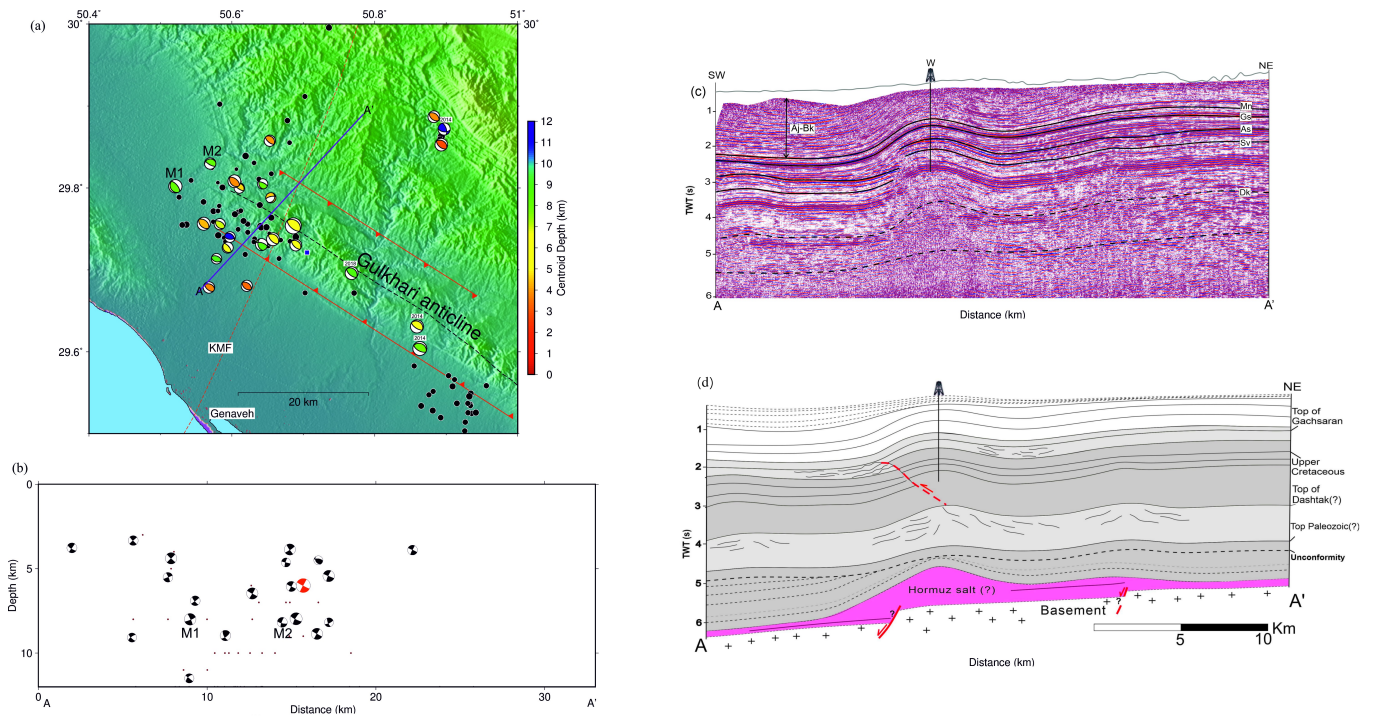


**Figure 3** a) Relocated epicenters (Black circles) of  $M_w \geq 3.0$  events and focal mechanisms of  $M_n \geq 4.0$  events colored by centroid depth. Four earthquake mechanisms labelled with years (2014, 2018) are background events and every other mechanism is an aftershock of the April 18,  $M_w$  5.9 Genaveh earthquake. The blue square shows the closest oil well to the seismic cluster. The Kharg-Mish Fault (KMF) and NW-SE trending blind thrust faults dipping NE and SW are shown by red lines. b) Cross section across the Gulkhari anticlines (A–A’ profile) with our calculated focal mechanisms at their centroid depths. The red mechanism presents the Genaveh mainshock. c) Interpreted seismic reflection profile (AA’ in panel a) across the Gulkhari anticline (Shamszadeh et al., 2022a). The y-axis is two-way travel time (TWT). Aj-Bk: Aghajari-Bakhtiyari formations, Mn: Mishan Formation, Gs: Gachsaran Formation, As: Asmari Formation, Sv: Sarvak Formation, and Dk: Dashtak Formation (for more information see figure S1). d) The interpreted 2D seismic profile of the Gulkhari anticline (after Shamszadeh et al., 2022a). The interpreted approximately NE-dipping reverse fault has an associated fold. The A–A’ seismic sections is presented in panel a. Panels (b),(c) and (d) are designed such that they have roughly equivalent vertical scales.

cut algorithm, unwrapping errors were then manually fixed. The fringes patterns obtained from InSAR consist of 4-5 fringes (Figure 5) that could be produced with a single fault plane either by a gently NE-dipping thrust fault or by a steeper SW-dipping one. To invert the ground displacements observed we followed routine elastic dislocation modeling procedures (Okada, 1985; Funning et al., 2005; Pousse-Beltran et al., 2020) in a half-space with elastic Lamé parameters  $\lambda = \mu = 2.5 \times 10^{10}$  Pa, to represent the sedimentary cover in which the fault is embedded (e.g. Nissen et al., 2010; Elliott et al., 2015; Jamalreyhani et al., 2021a). We derive the coseismic slip model in two steps: first, a uniform slip inversion with multiple Monte Carlo restarts (Wright et al., 1999), to search for the best fault geometry (position, strike, rake, dip, see Text S1, Figures S4, and S5), and secondly, we use this geometry to perform a slip distribution inversion. For the slip distribution inversion, we extended the model fault planes along the strike and up- and down-dip obtained in the first step, and we subdivided the extended fault plane into 1 km square patches (Figure 5). We also applied a Laplacian smoothing operator and assessed misfits using the L-curve criterion in order to determine the appropriate degree of smoothing (Funning et al., 2005; Wright et al., 2003). Ascending and descending data were weighted equally in the

inversion. We observe more residuals in the descending track, those positive residuals reaching 9.4 mm can be due to post-seismic displacements inverted as being recorded in the ascending track. Indeed the ascending interferogram spans 4 days more of the post-seismic period than the descending track.

The dip direction of the causative fault is ambiguous from the interferograms and both NE-dipping and SW-dipping model faults could reproduce the overall InSAR deformation pattern. But based on the mainshock and aftershock hypocentral locations, as well as the wide aftershock cloud (Figure 3), our preferred dip is the lower angle NE-dipping plane. This model also fits the InSAR data better than the other (RMS of  $5.8 \times 10^{-3}$  m here vs  $6.3 \times 10^{-3}$  m). The alternative SW-dipping model and a side-by-side comparison of the two models are shown in figures S6 and S7. Furthermore, the possible trade-off between parameters during the uniform inversion in both models is presented in figures S8 and S9. To consider the usual trade-off between slip and width, we repeat the inversion with slip fixed to an appropriate value for the  $M_w$  5.9 earthquake (e.g. 0.5 meters). We observed the high value of RMS and  $M_w$  for the SW-dipping model (Table S5 and Figure S10). In addition, when the slip is fixed, for the SW-dipping model, the dip is  $7^\circ$  higher ( $66^\circ$ ) and the fault plane is wider (Figure S10). Meanwhile, for

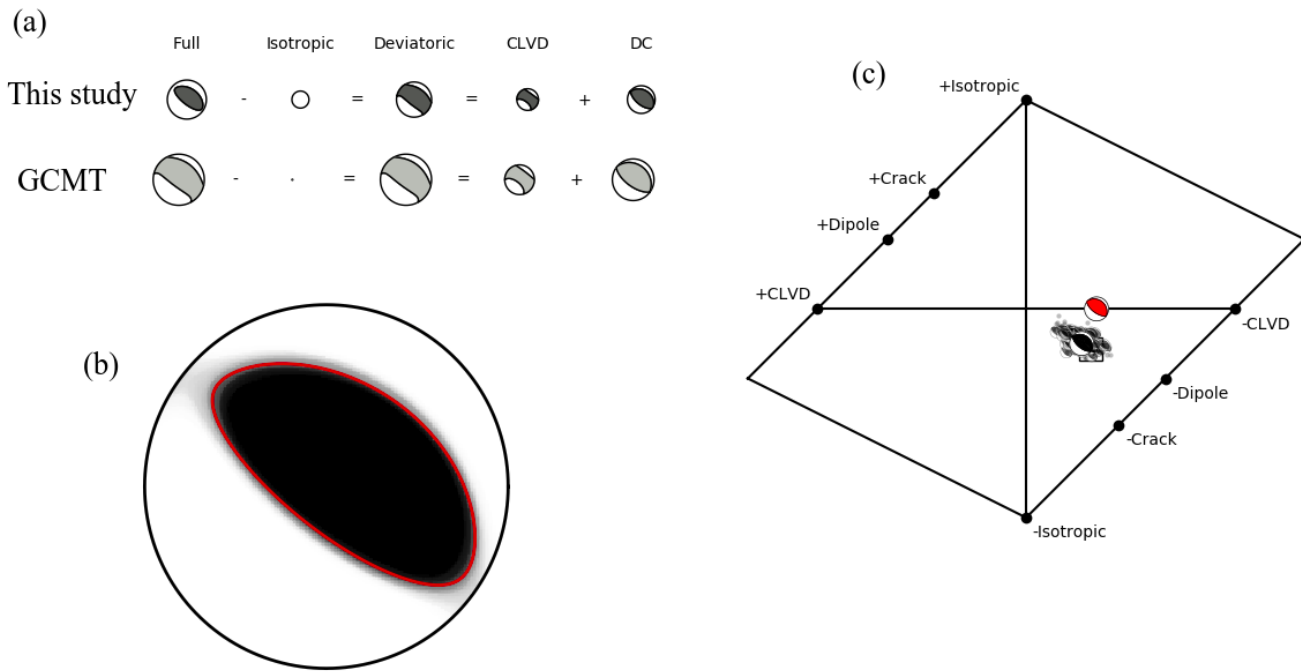


**Figure 4** a) Solution of full moment tensor inversion for the  $M_w$  5.9 Genaveh earthquake and decomposition of it in ISO, CLVD, and DC parts. The symbol size indicates the relative strength of the components. The Global Centroid Moment Tensor (GCMT) solution is shown for comparison. (b) The fuzzy full MT solution illustrates the uncertainty of the solution. (c) Hudson's source type plot with the ensemble of bootstrap solutions. The red mechanism shows the GCMT solution in the Hudson plot.

the NW-dipping fault model, solutions are similar.

The slip distribution model of the NE-dipping plane shows a slip mainly concentrated at depths of 5-6 km reaching 1m of slip. This distribution and amplitude depend on the degree of smoothing chosen according to the [Funning et al. \(2005\)](#) methodology. The InSAR model moment reaches  $1.104 \times 10^{18}$  Nm ( $M_w$  6.0) and yields an RMS of 0.00316 m. The hypocenter is located at the eastward limit and closer to the bottom of the slipping areas, likely indicating up-dip lateral rupture propagation toward NW.

### 3 Discussion

The  $M_w$  5.9 Genaveh earthquake occurred on 2021 April 18 in the SDE of ZFFB. The coseismic slip distribution of the Genaveh earthquake has been investigated by [Golshadi et al. \(2022\)](#) and [Jafari et al. \(2023\)](#) based on satellite data (see Table 2). [Golshadi et al. \(2022\)](#) suggested  $5.0 \times 9.5 \text{ km}^2$  for the fault plane and the fault top-edge depth at 4 km. Our obtained source geometry based on InSAR data conforms to their finding although we use a different downsampling methodology. There are differences between the results of [Golshadi et al. \(2022\)](#) and our study concerning slip depth, and the amount of maximum slip. [Golshadi et al. \(2022\)](#) obtained a maximum slip around 4.5 km depth, whereas we obtained a maximum slip at depths of 5-6 km. The localization of the [Golshadi et al. \(2022\)](#) fault is not clearly specified enough to compare. In addition, they obtained higher residuals above 10 mm. Furthermore, [Golshadi et al. 2020](#) and [Jafari et al., 2023](#) suggest the NE-dipping Zagros foredeep fault ([Berberian, 1995](#)) as a causative fault

for the Genaveh earthquake, however, our results show the shallow,  $\text{N}^{\text{W}}$ -trending, NE and SW dipping faults, located at both crest of the Gulkhari anticline and parallel to the trend of it, control the growth of this particular fold (Figure 3, e.g. M1, M2). Thus, we suggest the causative fault for the Genaveh earthquake mainshock is the gently NE-dipping Gulkhari fault, modeled through the InSAR technique and seismological observations. Our NE-dipping model fault has a strike of  $311^\circ$ , dips of  $20^\circ$ , and rake of  $96^\circ$ , conforming to the focal mechanism solution from waveform modeling ( $306^\circ$ ,  $28^\circ$ , and  $86^\circ$  for the strike, dip, and rake, respectively). The InSAR model moment is higher than the seismic moment ( $M_w$  5.9), though it is possible that our InSAR models also include a small amount of postseismic afterslip. This solution is also coherent with other published source models (see Table 2). Our results show minimum RMS with a top depth around 4-5 km and a bottom depth around 5.5-6.5 km (Figure S8). This supports the slip localization around 5-6 km depth in our slip distributed inversion and at the same depth range determined by moment tensor inversion (Figure S3).

We additionally assess the aftershock sequence and calculate their focal mechanisms by waveform modeling. Locations and mechanisms of the aftershock sequence are very useful to understand the on/off fault seismicity, the process of mainshock rupture, and post-seismic deformation ([Das and Henry, 2003](#)). The relocation of the Genaveh earthquake sequence, which was recorded by newly installed stations by the IRSC network, helped to partly complement the existing data gap in the South Dezful Embayment in [Karasözen et al. \(2019\)](#) study which was due to poor station coverage.

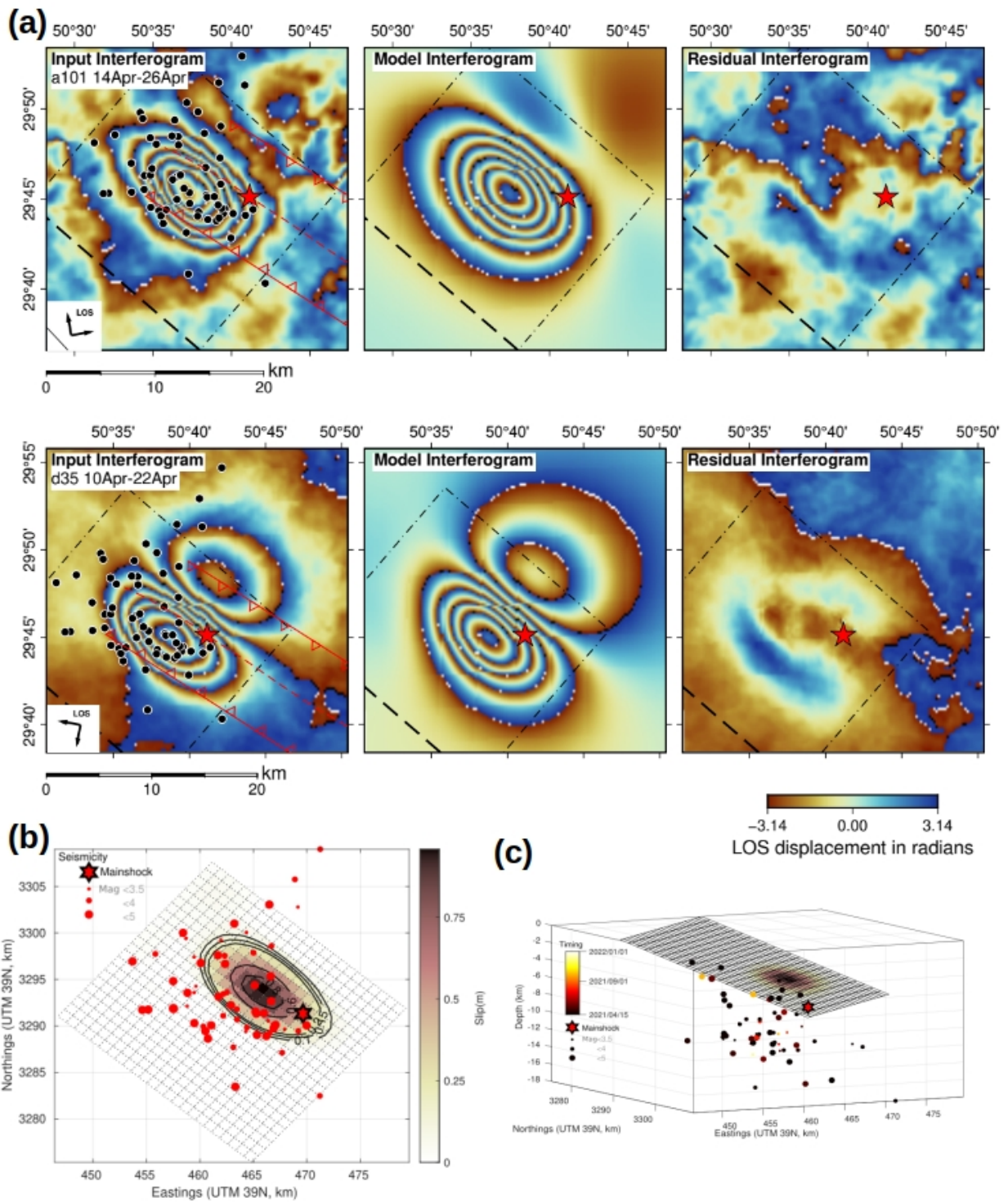


**Figure 5** Coseismic slip distribution inversion results. (a) The first and second rows correspond, respectively, to the ascending track A101 and the descending track D35. From left to right columns: observed, model, and residual interferograms. Results are shown re-wrapped. The red star is the relocated epicenter of the mainshock. Black dots are the relocated aftershocks. The bold black dashed line corresponds to the surface projection of the modeled faults. The black dashed dotted rectangle corresponds to the projection of the modeled fault plane. The Kharg-Mish Fault (KMF) and NW-SE trending blind thrust faults dipping NE and SW are shown by red lines. (b) Coseismic slip distribution in map view, the model fault is divided by a  $1 \text{ km}^2$  patch. The red star is the relocated epicenter, dots show the relocated aftershocks. (c) Coseismic slip distribution in 3D, dots shows the relocated aftershocks colored according to time.

The aftershock focal mechanisms and their distribution suggest that some of the aftershocks take place on the same fault plane as the Genaveh mainshock, but some are also distributed along the ~NW-trending, SW dip-

ping fault, located at the northern crest of the Gulkhari anticline (Figure 3), likely the consequence of mainshock and bending stresses within the layers of the fold, which highlights the role of fault structure and rheology

Track	Date 1	Date 2	LOS incidence (°)	LOS azimuth (°)
A101	14 Apr. 2021	26 Apr. 2021	42	77
D035	10 Apr. 2021	22 Apr. 2021	35	-77

**Table 1** InSAR interferogram characteristic used in this study (A: Ascending, D: Descending, LOS: Line of Sight). Incidence and azimuth angles are measured at the epicenter.

Method	Source	Magnitude ( $M_w$ )	Strike (°)	Dip (°)	Rake (°)	Depth (km)	Max Slip (m)
InSAR	Golshadi et al., (2022)	5.9	313	20	100	4	1
InSAR	Jafari et al., (2023)	5.8	306	23	89	6	0.95
InSAR	This study	6	311	20	96	4-7	1
Waveform modeling	This study	5.9	$306 \pm 5$	$28 \pm 9$	$86 \pm 10$	$6.0 \pm 2.0$	-

**Table 2** Source parameters of the 2021 Genaveh earthquake obtained in this study, Golshadi et al. (2022) and Jafari et al. (2023) based on InSAR and seismological models.

in controlling the distribution of seismicity (e.g. Collet-tini et al., 2022). Furthermore, this displays the correlation between the Gulkhari anticline and the seismogenic thrust and reverse faults beneath it.

The focal solution and location of the background seismicity which are spatially away from the mainshock and localized in the southern part of the Gulkhari anticline (Figures 2 and 3), demonstrate that the southern part of the NE dipping Gulkhari fault was seismically active (Two events occurred on 21 April 2014 within the magnitude of  $M_w$  5.3 and 5.1, and an event in March 2018,  $M_w$  5.0). The Genaveh earthquake is spatially localized in the northern part of the Gulkhari anticline.

The MT inversion of the mainshock shows a centroid depth of  $6 \pm 2$  km. Focal mechanisms represent a regional transpressional tectonic regime (maximum horizontal stress,  $\sigma_1$ ) oriented axis at  $\sim N45E$  (Heidbach et al., 2018), and are compatible with the principal stress axis of the region. From InSAR modeling, we obtained the depth of a large slip area of about 5 km. Considering the low dip angle of the modeled fault (from both focal mechanism and finite fault modeling), the rupture occurred in the competent group (Sherkati et al., 2005; Nissen et al., 2011) of sedimentary cover. It is probable that the incompetent layers limit the rupture to propagate and generate large magnitudes ( $M_w$  6+) of shock. Likely, the rupture deepest part is affected by the Paleozoic Shale layer, which makes the rupture fail to propagate and highlights the influence of lithology in the rupture propagation. Furthermore, the top depth of the ruptured area confines at the depth of  $\sim 3-4$  km, corresponding to the depth of the upper mobile group. Moreover, the presence of an NE dipping fault is clear in the seismic section and it has grown in between Gachsaran and Dashtak layers (Figure 3). This explains top and bottom depths corresponding to detachments in weak evaporitic layers that act to limit up- and down-dip rupture propagation and thus, restrict the magnitude. Also, none of the aftershock centroid depths are less than  $\sim 3$  km. There are no large instrumental earthquakes exceeding  $M_w$  6 in the Dezful Embayment, showing that the seismogenic layer is segmented by weak evaporitic within the sedimentary cover, and controls the propagation of earthquake rupture, similar to the Fars arc (Nissen et al., 2010; Jamalreyhani et al., 2021a).

There are very few thrust-faulting earthquakes in the Fars arc of ZFFB with significantly large magnitudes (Nissen et al., 2011). Clearly, at the base of the cover, the Hormuz salt plays a role and barriers the rupture propagation in the Fars arc. The most moderate-sized event ( $5 < M_w < 6$ ) in the ZFFB occurs within the mid-lower sedimentary cover (Nissen et al., 2007, 2010; Roustaei et al., 2010; Copley et al., 2015; Motagh et al., 2015). In the Dezful Embayment, the presence of the Hormuz salt layer is debated. Nonetheless, in the Gulkhari anticline, the seismic profile displays a salt-cored structure within slight vergence to the SW, which is detached from the Hormuz salt layers (Shamszadeh et al., 2022a). Therefore, this may be controlled by other weak evaporitic or shale horizons within the cover and also reflect the narrow (small width-to-length ratio) dimensions, as observed in the Genaveh coseismic slip. In the middle and upper parts of the cover, there are for example Gurpi marls and Gachsaran evaporites to play a barrier role. Aftershocks of the Genaveh earthquake lie within the sedimentary cover too, there is no observation of vertical separation for this cluster. Meanwhile, a detailed micro-aftershocks study would be required to discuss this, which is beyond the data resolution of this study.

The Genaveh earthquake is co-located with the major Gulkhari oil reservoir at the Asmari-Jahrum formation and raised the question about the possible involvement of the oil extraction in the field and this earthquake. However, human actions only affect the uppermost several kilometers of the crust, and the induced earthquakes are expected to occur at shallow depths (Dahm et al., 2015; Cesca et al., 2021). Hence, depth is a particularly important discriminator between anthropogenic and natural seismicity in the Zagros (Jamalreyhani et al., 2021a). The depth of the Genaveh seismic sequence is in the typical earthquake depth range in the Zagros and does not support an induced earthquake related to the oil field (oil extraction starting in 1987 with 15,000 barrels per day), which is deeper than the oil reservoir's depth ( $\sim 4$  km). Although, the full moment tensor of the mainshock, suggests a notable non-DC component (Figure 4) and may reflect the source complexity (Dahm et al., 2015; Wang et al., 2018). The sequence also depicts typical mainshock-aftershock patterns and focal mechanisms represent-

ing reverse/thrust faulting, compatible with regional tectonic stresses and corresponding to the previously known fault(s). Furthermore, the Genaveh earthquake is spatially localized in the northern part of the Gulkhari anticline, which is outward of the location of extraction/injection wells (Figure 3). Therefore, detailed sophisticated production data in the Gulkhari oil field is required to track the relationship between oil extraction and seismic activity in the past and future.

## 4 Conclusion

We present a detailed analysis of the  $M_w$  5.9 Genaveh earthquake on 2021 April 18 as a well-recorded example of seismic activity in the South Dezful Embayment of Zagros foreland folded belt. We analyzed the Genaveh earthquake sequence using local and regional seismic data and constrained the co-seismic slip of the mainshock with InSAR modeling. Coseismic uplift in the Gulkhari anticline shows the surface configuration of this fold, reflecting subsurface structural conditions. This earthquake involved a gently ( $\sim 20^\circ$ ) NE-dipping fault plane (named Gulkhari fault). The main slip of the mainshock was restricted to depths of between 4–7 with a maximum slip of 1 m within the sedimentary cover which highlights the influence of lithology in the rupture propagation. Aftershocks of the Genaveh earthquake are widely distributed and dominated by reverse faulting at centroid depths of 4–10 km.

Although the Genaveh earthquake is co-located with the major Gulkhari oil reservoir, the detailed relationship between the oil extraction in the field and this earthquake needs sophisticated data to investigate, though, our results support the essence of a tectonic earthquake.

## Acknowledgements

We thank all data research centers for providing the data used in this study. We thank Isapron Sethanant for sharing the plotting codes. We appreciate the Seismica community that supports open-access publishing in seismology and earthquake science. We would like to thank E. Nissen and an anonymous reviewer for their careful reviews, the associate editor G. Funning, and editor Y.J. Tan for their comments and for handling the manuscript.

## Data and code availability

All data used in this study is freely available. The seismic catalog and waveforms of the Iran network were downloaded from the Iranian Seismological Center (IRSC) available at <http://irsc.ut.ac.ir/>. InSAR interferograms were made using Copernicus Sentinel data (<https://scihub.copernicus.eu/>).

The nonlinear inversion code of moment tensors is all provided by the Pyrocko (Heimann et al., 2017) seismology toolbox and library (<https://pyrocko.org>). The relocation software (The MLOC program Bergman

et al., 2022) is available at <https://seismo.com/mloc/>. InSAR data were processed using the online service GDM-SAR (<https://www.poleterresolide.>) supported by Formater (<https://www.poleterresolide.>), CNES (<https://cnes.fr/fr>) and the European Union's Caroline Herschel Framework Partnership Agreement on Copernicus User Uptake under grant agreement No FPA 275/G/GRO-COPE/17/10042, project FPCUP (Framework Partnership Agreement on Copernicus User Uptake), Action 2019-1-39 "Promote the use of COPERNICUS Sentinel-1 data and valorize a prototype of an on-demand service for radar interferometry processing". For the InSAR inversion, we used the codes developed by the Centre for the Observation and Modelling of Earthquakes, Volcanoes, and Tectonics (COMET) group (<https://comet.nerc.ac.uk/>) (Wright et al., 1999; Funning et al., 2005) available from request.

The InSAR unwrapped data, the result of the quadtree sampling, and the two slip distribution models are stored in this link: <https://zenodo.org/record/7148513> and can be downloaded anonymously.

## Competing interests

The authors declare that they have no known competing financial interests or personal relationships that could have appeared to influence the work reported in this paper.

## References

- Abdollahie Fard, I., Sepehr, M., and Sherhati, S. Neogene salt in SW Iran and its interaction with Zagros folding. *Geological Magazine*, 148(5-6):854–867,, 2011. doi: 10.1017/S0016756811000343.
- Alavi, M. Structures of the Zagros Fold-Thrust Belt in Iran. *American Journal of Science*, 308(1):104–104, 2008. doi: 10.2475/01.2008.05.
- Allen, M. and Talebian, M. Structural variation along the Zagros and the nature of the Dezful Embayment. *Geological Magazine*, 148:911–924,, 2011. doi: 10.1017/S0016756811000318.
- Ambraseys, N. and Melville, C. *A history of Persian earthquakes*. Cambridge University Press, 1982.
- Berberian, M. Master "blind" thrust faults hidden under the Zagros folds: Active basement tectonics and surface morphotectonics. *Tectonophysics*, 241(3):193–224,, 1995. doi: 10.1016/0040-1951(94)00185-C.
- Bergman, E., Benz, H., Yeck, W., Karasözen, E., Engdahl, E., Ghods, A., Hayes, G., and Earle, P. A Global Catalog of Calibrated Earthquake Locations. *Seismological Research Letters*, 2022. doi: 10.1785/0220220217.
- Büyükkapınar, P., Cesca, S., Hainzl, S., Jamalreyhani, M., Heimann, S., and Dahm, T. Reservoir-Triggered Earthquakes Around the Atatürk Dam (Southeastern Turkey). *Frontiers in Earth Sciences*, 9, 2021. doi: 10.3389/feart.2021.663385.
- Carruba, S., Perotti, C., Buonaguro, R., Calabrò, R., Carpi, R., and Naini, M. Structural pattern of the Zagros fold-and-thrust belt in the Dezful Embayment (SW Iran). In Mazzoli, S. and Butler, R., editors, *Styles of Continental Contraction: Geological Society of America Special Paper 414*, pages 11–32,, 2006. doi: 10.1130/2006.2414(02).

- Cesca, S., Stich, D., Grigoli, F., Vuan, A., López-Comino, J., Niemi, P., Blanch, E., Dahm, T., and Ellsworth, W. Seismicity at the Castor gas reservoir driven by pore pressure diffusion and asperities loading. *Nature communications*, 12:4783, 2021. doi: 10.1038/s41467-021-24949-1.
- Collettini, C., Barchi, M., Paola, N., Trippetta, F., and Tinti, E. Rock and fault rheology explain differences between on fault and distributed seismicity. *Nature communications*, 13:5627, 2022. doi: 10.1038/s41467-022-33373-y.
- Copley, A., Karasozen, E., Oveisi, B., Elliott, J., Samsonov, S., and Nissen, E. Seismogenic faulting of the sedimentary sequence and laterally variable material properties in the Zagros Mountains (Iran) revealed by the August 2014 Murmuri (E. Dehloran) earthquake sequence. *Dehloran earthquake sequence. Geophysical Journal International*, 203:1436–1459, 2015. doi: 10.1093/gji/ggv365.
- Dahm, T., Cesca, S., Hainzl, S., Braun, T., and Krüger, F. Discrimination between induced, triggered, and natural earthquakes close to hydrocarbon reservoirs: A probabilistic approach based on the modeling of depletion-induced stress changes and seismological source parameters. *Journal of Geophysical Research: Solid Earth*, 120:2491–2509, 2015. doi: 10.1002/2014JB011778.
- Das, S. and Henry, C. Spatial relation between main earthquake slip and its aftershock distribution. *Reviews of Geophysics*, 41, 2003. doi: 10.1029/2002RG000119.
- Donner, S., Igel, H., Hadziioannou, C., and the Romy group. Retrieval of the Seismic Moment Tensor from Joint Measurements of Translational and Rotational Ground Motions: Sparse Networks and Single Stations. In D'Amico, S., editor, *Moment Tensor Solutions: A Useful Tool for Seismotectonics*, pages 263–280. Springer Natural Hazards. Springer International Publishing, Cham, 2018. doi: [https://doi.org/10.1007/978-3-319-77359-9\\_12](https://doi.org/10.1007/978-3-319-77359-9_12).
- Elliott, J., Bergman, E., Copley, A., Ghods, A., Nissen, E., Oveisi, B., Tatar, M., Walters, R., and Yamini-Fard, F. The 2013 Mw 6.2 Khaki-Shonbe (Iran) Earthquake: Insights into seismic and aseismic shortening of the Zagros sedimentary cover. *Earth and Space Science*, 2:435–471, 2015. doi: 10.1002/2015EA000098.
- Farahzadi, E., Alavi, S., Sherkat, S., and Ghassemi, M. Variation of subsidence in the Dezful Embayment, SW Iran: influence of reactivated basement structures. *Arabian Journal of Geosciences*, 12:616, 2019. doi: 10.1007/s12517-019-4758-5.
- Funning, G., Parsons, B., Wright, T., Jackson, J., and Fielding, E. Surface displacements and source parameters of the 2003 Bam (Iran) earthquake from Envisat advanced synthetic aperture radar imagery. *Journal of Geophysical Research: Solid Earth*, 110(B9), 2005. doi: 10.1029/2004JB003338.
- Golshadi, Z., Famiglietti, N., Atzori, S., and Vicari, A. Surface Displacement and Source Parameters of the 2021 Bandar-e Genaveh, Iran, Earthquake Determined from InSAR Observations. *Applied Sciences*, 12:4223, 2022. doi: 10.3390/app12094223.
- Heidbach, O., Rajabi, M., Cui, X., Fuchs, K., Müller, B., Reinecker, J., Reiter, K., Tingay, M., Wenzel, F., Xie, F., Ziegler, M., Zoback, M.-L., and Zoback, M. The World Stress Map database release 2016: Crustal stress pattern across scales. *Tectonophysics*, 744: 484–498, 2018. doi: 10.1016/j.tecto.2018.07.007.
- Heimann, S., Kriegerowski, M., Isken, M., Cesca, S., Daout, S., Grigoli, F., Juretzek, C., Megies, T., Nooshiri, N., Steinberg, A., Sudhaus, H., Vasyura-Bathke, H., Willey, T., and Dahm, T. Pyrocko - An open-source seismology toolbox and library, 2017. doi: 10.5880/GFZ.2.1.2017.001, GFZ Data Services.
- Heimann, S., Vasyura-Bathke, H., Sudhaus, H., Isken, M., Kriegerowski, M., Steinberg, A., and Dahm, T. A Python framework for efficient use of pre-computed Green's functions in seismological and other physical forward and inverse source problems. *Solid Earth*, 10:1921–1935, 2019. doi: 10.5194/se-10-1921-2019.
- Irandoost, M., Priestley, K., and Sobouti, F. High-Resolution Lithospheric Structure of the Zagros Collision Zone and Iranian Plateau. *Journal of Geophysical Research: Solid Earth*, 127, 2022. doi: 10.1029/2022JB025009.
- Jafari, M., Aflaki, M., Mousavi, Z., Walpersdorf, A., and Motaghi, K. Coseismic and postseismic characteristics of the 2021 Ganaveh earthquake along the Zagros foredeep fault based on InSAR data. *Geophysical Journal International*, 2023. doi: 10.1093/gji/ggad127.
- Jahani, S., Callot, J., Letouzey, J., and Lamotte, D. The eastern termination of the Zagros Fold-and-Thrust Belt, Iran: Structures, evolution, and relationships between salt plugs, folding, and faulting. *Tectonics*, 28(6), 2009. doi: 10.1029/2008TC002418.
- Jahani, S., Hassanpour, J., Mohammadi-Firouz, S., Letouzey, J., Lamotte, D., Alavi, S., and Soleimany, B. Salt tectonics and tear faulting in the central part of the Zagros Fold-Thrust Belt, Iran. *Marine and Petroleum Geology*, 86:426–446, 2017. doi: 10.1016/j.marpetgeo.2017.06.003.
- Jamalreyhani, M., Rezapour, M., Cesca, S., Heimann, S., Vasyura-Bathke, H., Sudhaus, H., Isken, M., and Dahm, T. The 2017 November 12 Mw 7.3 Sarpol-Zahab (Iran-Iraq border region) earthquake: source model, aftershock sequence and earthquakes triggering. EGU2020 Copernicus Meetings, EGU2020-759, 2019. doi: 10.5194/egusphere-egu2020-759.
- Jamalreyhani, M., Büyükkakpınar, P., Cesca, S., Dahm, T., Sudhaus, H., Rezapour, M., Isken, M. P., Maleki Asayesh, B., and Heimann, S. Seismicity related to the eastern sector of Anatolian escape tectonic: the example of the 24 January 2020 Mw 6.77 Elazığ-Sivrice earthquake. *Solid Earth Discussions*, 2020:1–22, 2020. doi: 10.5194/se-2020-55.
- Jamalreyhani, M., Pousse-Beltran, L., Büyükkakpınar, P., Cesca, S., Nissen, E., Ghods, A., López-Comino, J., Rezapour, M., and Najafi, M. The 2019–2020 Khalili (Iran) Earthquake Sequence—Anthropogenic Seismicity in the Zagros Simply Folded Belt? *Journal of Geophysical Research: Solid Earth*, 126, 2021a. doi: 10.1029/2021JB022797.
- Jamalreyhani, M., Rezapour, M., and Büyükkakpınar, P. Evaluation of seismic sensor orientations in the full moment tensor inversion results, 2021b. doi: 10.5194/egusphere-egu21-459, EGU21 Copernicus Meetings, EGU21-459.
- Jamalreyhani, M., Rezapour, M., Cesca, S., Dahm, T., Heimann, S., Sudhaus, H., and Isken, M. Insight into the 2017–2019 Lurestan arc seismic sequence (Zagros, Iran); complex earthquake interaction in the basement and sediments. *Geophysical Journal International*, 2022. doi: 10.1093/gji/ggac057.
- Karasözen, E., Nissen, E., Bergman, E., and Ghods, A. Seismotectonics of the Zagros (Iran) From Orogen-Wide, Calibrated Earthquake Relocations. *Journal of Geophysical Research: Solid Earth*, 124:9109–9129, 2019. doi: 10.1029/2019JB017336.
- McQuarrie, N. Crustal scale geometry of the Zagros fold-thrust belt. *Iran, Journal of Structural Geology*, 26:519–535, 2004. doi: 10.1016/j.jsg.2003.08.009.
- Motagh, M., Bahroudi, A., Haghghi, M. H., Samsonov, S., Fielding, E., and Wetzel, H. The 18 August 2014 Mw 6.2 Mormori, Iran, Earthquake: A Thin-Skinned Faulting in the Zagros Mountain Inferred from InSAR Measurements. *Seismological Research Letters*, 86(3):775–782, 04 2015. doi: 10.1785/0220140222.
- Mouthereau, F., Tensi, J., Bellahsen, N., Lacombe, O., De Boisgrollier, T., and Kargar, S. Tertiary sequence of deformation in a thin-skinned/thick-skinned collision belt: The Zagros

- Folded Belt (Fars, Iran). *Tectonics*, 26(5), 2007. doi: <https://doi.org/10.1029/2007TC002098>.
- Mouthereau, F., Lacombe, O., and Vergés, J. Building the Zagros collisional orogen: Timing, strain distribution and the dynamics of Arabia/Eurasia plate convergence. *Tectonophysics*, 532–535: 27–60,, 2012. doi: [10.1016/j.tecto.2012.01.022](https://doi.org/10.1016/j.tecto.2012.01.022).
- Najafi, M. and Lajmorak, S. Contractional salt-tectonic system in the south Dezful embayment, Zagros. *Journal of Structural Geology*, 141:104204,, 2020. doi: [10.1016/j.jsg.2020.104204](https://doi.org/10.1016/j.jsg.2020.104204).
- Najafi, M., Yassaghi, A., Bahroudi, A., Vergés, J., and Sherkati, S. Impact of the Late Triassic Dashtak intermediate detachment horizon on anticline geometry in the Central Frontal Fars, SE Zagros fold belt, Iran. *Marine and Petroleum Geology*, 54:23–36,, 2014. doi: [10.1016/j.marpetgeo.2014.02.010](https://doi.org/10.1016/j.marpetgeo.2014.02.010).
- Nissen, E., Ghorashi, M., Jackson, J., Parsons, B., and Talebian, M. The 2005 Qeshm Island earthquake (Iran)—a link between buried reverse faulting and surface folding in the Zagros Simply Folded Belt? *Geophysical Journal International*, 171(1):326–338, 10 2007. doi: [10.1111/j.1365-246X.2007.03514.x](https://doi.org/10.1111/j.1365-246X.2007.03514.x).
- Nissen, E., Yamini-Fard, F., Tatar, M., Gholamzadeh, A., Bergman, E., Elliott, J., Jackson, J., and Parsons, B. The vertical separation of mainshock rupture and microseismicity at Qeshm island in the Zagros fold-and-thrust belt, Iran. *Earth and Planetary Science Letters*, 296(3):181–194, 2010. doi: <https://doi.org/10.1016/j.epsl.2010.04.049>.
- Nissen, E., Tatar, M., Jackson, J., and Allen, M. New views on earthquake faulting in the Zagros fold-and-thrust belt of Iran. *Geophysical Journal International*, 186(3):928–944,, 2011. doi: [10.1111/j.1365-246X.2011.05119.x](https://doi.org/10.1111/j.1365-246X.2011.05119.x).
- Nissen, E., Ghods, A., Karasözen, E., Elliott, J., Barnhart, W., Bergman, E., Hayes, G., Jamal-Reyhani, M., Nemati, M., Tan, F., Abdalnaby, W., Benz, H., Shahvar, M., Talebian, M., and Chen, L. The 12 November 2017  $M_w$  7.3 Ezgeleh-Sarpolzahab (Iran). *Earthquake and Active Tectonics of the Lurestan Arc. Journal of Geophysical Research: Solid Earth*, 124:2124–2152,, 2019. doi: [10.1029/2018JB016221](https://doi.org/10.1029/2018JB016221).
- Okada, Y. Surface deformation due to shear and tensile faults in a half-space. *Bulletin of the seismological society of America*, 75 (4):1135–1154,, 1985. doi: [10.1785/BSSA0750041135](https://doi.org/10.1785/BSSA0750041135).
- Pousse-Beltran, L., Nissen, E., Bergman, E., Cambaz, M., Gaudreau, E., Karasözen, E., and Tan, F. The 2020  $M_w$  6.8 Elazığ (Turkey) earthquake reveals rupture behavior of the East Anatolian Fault. *Geophysical Research Letters*, 47(13), 2020. doi: [10.1029/2020GL088136](https://doi.org/10.1029/2020GL088136).
- Roustaei, M., Nissen, E., Abbassi, M., Gholamzadeh, A., Ghorashi, M., Tatar, M., Yamini-Fard, F., Bergman, E., Jackson, J., and Parsons, B. The 2006 March 25 Fin earthquakes (Iran)—insights into the vertical extents of faulting in the Zagros Simply Folded Belt. *Geophysical Journal International*, 181:1275–1291,, 2010. doi: [10.1111/j.1365-246X.2010.04601.x](https://doi.org/10.1111/j.1365-246X.2010.04601.x).
- Sepehr, M. and Cosgrove, J. Structural framework of the Zagros Fold–Thrust Belt, Iran. *Marine and Petroleum Geology*, 21(7):829–843, 2004. doi: <https://doi.org/10.1016/j.marpetgeo.2003.07.006>.
- Seraj, M., Faghih, A., Motamedi, H., and Soleimany, B. Major Tectonic Lineaments Influencing the Oilfields of the Zagros Fold-Thrust Belt, SW Iran: Insights from Integration of Surface and Subsurface Data. *Journal of Earth Science*, 31:596–610,, 2020. doi: [10.1007/s12583-020-1303-0](https://doi.org/10.1007/s12583-020-1303-0).
- Shamszadeh, A., Sarkarinejad, K., Ferrer, O., Mukherjee, S., and Seraj, M. Effect of inherited structural highs on the structure and kinematics of the South Dezful Embayment, SW Iran. *Geological Magazine*, pages 1–23,, 2022a. doi: [10.1017/S0016756822000541](https://doi.org/10.1017/S0016756822000541).
- Shamszadeh, A., Sarkarinejad, K., Ferrer, O., Mukherjee, S., and Seraj, M. Interaction of inherited structures and contractional deformation in the South Dezful Embayment: Insights from the Gachsaran oilfield, SW Iran. *Marine and Petroleum Geology*, 145: 105871,, 2022b. doi: [10.1016/j.marpetgeo.2022.105871](https://doi.org/10.1016/j.marpetgeo.2022.105871).
- Sherkati, S. and Letouzey, J. Variation of structural style and basin evolution in the central Zagros (Izeh zone and Dezful Embayment). *Iran. Marine and Petroleum Geology*, 21:535–554,, 2004. doi: [10.1016/j.marpetgeo.2004.01.007](https://doi.org/10.1016/j.marpetgeo.2004.01.007).
- Sherkati, S., Molinaro, M., Lamotte, D., and Letouzey, J. Detachment folding in the Central and Eastern Zagros fold-belt (Iran): salt mobility, multiple detachments and late basement control. *Journal of Structural Geology*, 27:1680–1696,, 2005. doi: [10.1016/j.jsg.2005.05.010](https://doi.org/10.1016/j.jsg.2005.05.010).
- Sherkati, S., Letouzey, J., and Frizon de Lamotte, D. Central Zagros fold-thrust belt (Iran): New insights from seismic data, field observation, and sandbox modeling. *Tectonics*, 25(4), 2006. doi: <https://doi.org/10.1029/2004TC001766>.
- Stöcklin, J. Structural History and Tectonics of Iran1: A Review. *AAPG Bulletin*, 52:1229–1258,, 1968. doi: [10.1306/5D25C4A5-16C1-11D7-8645000102C1865D](https://doi.org/10.1306/5D25C4A5-16C1-11D7-8645000102C1865D).
- Talebian, M. and Jackson, J. A reappraisal of earthquake focal mechanisms and active shortening in the Zagros mountains of Iran. *Geophysical Journal International*, 156(3):506–526,, 2004. doi: [10.1111/j.1365-246X.2004.02092.x](https://doi.org/10.1111/j.1365-246X.2004.02092.x).
- Tourani, M., Isik, V., Saber, R., and Caglayan, A. Radar Interferometric Assessment of April 18, 2021 Bandar Ganaveh Earthquake ( $m_w$ : 5.8). In *Southern Iran. Presented at the 11th Congress of the Balkan Geophysical Society, European Association of Geoscientists and Engineers*, pages 1–5,. 2021. doi: [10.3997/2214-4609.202149BGS89](https://doi.org/10.3997/2214-4609.202149BGS89).
- Vergés, J., Saura, E., Casciello, E., Fernández, M., Villaseñor, A., Jiménez-Munt, I., and García-Castellanos, D. Crustal-scale cross-sections across the NW Zagros belt: implications for the Arabian margin reconstruction. *Geological Magazine*, 148: 739–761,, 2011. doi: [10.1017/S0016756811000331](https://doi.org/10.1017/S0016756811000331).
- Walker, R., Bergman, E., Szeliga, W., and Fielding, E. Insights into the 1968–1997 Dasht-e-Bayaz and Zirkuh earthquake sequences, eastern Iran, from calibrated relocations, InSAR and high-resolution satellite imagery. *Geophysical Journal International*, 187:1577–1603,, 2011. doi: [10.1111/j.1365-246X.2011.05213.x](https://doi.org/10.1111/j.1365-246X.2011.05213.x).
- Wang, R., Gu, Y., Schultz, R., and Chen, Y. Faults and Non-Double-Couple Components for Induced Earthquakes. *Geophysical Research Letters*, 45:8966–8975,, 2018. doi: [10.1029/2018GL079027](https://doi.org/10.1029/2018GL079027).
- Wang, S., Nissen, E., Pousse-Beltran, L., Craig, T., Jiao, R., and Bergman, E. Structural controls on coseismic rupture revealed by the 2020  $M_w$  6.0 Jiashi earthquake (Kepingtag belt, SW Tian Shan, China). *Geophysical Journal International*, 2022. doi: [10.1093/gji/ggac159](https://doi.org/10.1093/gji/ggac159).
- Wright, T., Parsons, B., Jackson, J., Haynes, M., Fielding, E., England, P., and Clarke, P. Source parameters of the 1 October 1995 Dinar (Turkey) earthquake from SAR interferometry and seismic bodywave modelling. *Earth and Planetary Science Letters*, 172: 23–37,, 1999. doi: [10.1016/S0012-821X\(99\)00186-7](https://doi.org/10.1016/S0012-821X(99)00186-7).
- Wright, T., Lu, Z., and Wicks, C. Source model for the  $M_w$  6.7, 23 October 2002, Nenana Mountain Earthquake (Alaska) from InSAR. *Geophysical Research Letters*, 30(18), 2003. doi: [10.1029/2003GL018014](https://doi.org/10.1029/2003GL018014).
- Yaghoobi, A., Mahbaz, S., Dusseault, M. B., and Leonenko, Y. Seismicity and the State of Stress in the Dezful Embayment, Zagros Fold and Thrust Belt. *Geosciences*, 11(6), 2021. doi: [10.3390/geosciences11060254](https://doi.org/10.3390/geosciences11060254).

Zahradnik, J., Jansky, J., and Plicka, V. Detailed Waveform Inversion for Moment Tensors of  $M \sim 4$  Events: Examples from the Corinth Gulf, Greece. *Bulletin of the Seismological Society of America*, 98:2756–2771, 2008. doi: 10.1785/0120080124.

The article *Co-seismic slip of the 18 April 2021  $M_w$  5.9 Genaveh earthquake in the South Dezful Embayment of Zagros (Iran) and its aftershock sequence* © 2023 by M. Jamalreyhani is licensed under CC BY 4.0.